Precision Engineering 84 (2023) 45–55

Contents lists available at ScienceDirect

Precision Engineering

journal homepage: www.elsevier.com/locate/precision

Pneumatics can be precise - Methodology of building a stand with high repeatability for calibrating measuring arms

Adam Bryszewski, Jakub Głowacki, Piotr Zgórniak, Leszek Podsędkowski, Agnieszka Kobierska *

Lodz University of Technology, Poland

ARTICLE INFO

Handling Editor: Dr. S Ludwick

Keywords:
Stewart platform
Measuring arm
Calibration
High repeatability

ABSTRACT

This paper presents the process of designing a highly repeatable calibration station for the NaviFast 6D measuring arm. This is a new solution, characterized by repeatability at the level of 1 μm for access from one direction, the ability to change the setting of the base and effector of the arm, fully automatic measurement, and relatively low construction cost. In this solution, human error has been eliminated as much as possible. The stand consists of two Stewart platforms equipped with double-acting pneumatic actuators on which the calibration arm is placed. The stand is able to provide 4096 different positions – a sufficient number for calibrating the arms. In addition, the paper presents the methodology of designing stations for various types of measuring arms and the methodology of selecting parameters for the appropriate working space of a measuring arm.

1. Introduction

1.1. State of art

Participation of robots in every aspect of life is subject to an increase every year. This is due to the need to automate processes and the resulting lower probability of making mistakes. One branch of robotics that is growing increasingly is measuring manipulators. These are certain types of robots or passive manipulators, usually in series, that are used to measure the shape and dimensions of workpieces in a manufacturing process. An important activity with measuring arms is to calibrate them. This is quite an extensive topic and depends largely on the type of measuring manipulator.

One of the most common methods of calibration is calibration on a sphere, a cone, or on multiple spheres separated from each other by a certain calibrated value. This is described in the standard [1]. Care must be taken in this method to ensure that the test sphere and the coordinate measuring arm are rigidly fixed. This is important to minimize deflection and backlash as much as possible. Measurement on one sphere is made at 5 points from different directions (4 points are located on the four quadrants of the sphere, and the fifth point is at a location that is symmetrical with respect to the other four). Moreover, four additional points are measured for each direction without changing the direction of the stylus. In such situations, the calibration procedure provides only one piece of information per measurement - the position of the contact surface in the direction along the radius of the sphere located at the end of the stylus at the point of contact.

The method of calibration on a sphere is developed with additional calibration of length measurement. Evaluation of the error is based on the use of calibrated workpieces of a specific length. Five length standards are used. The longest workpiece should have a length equal to about 66% of the measuring range of the arm. The workpieces are then measured in three positions on one plane (horizontal, vertical, 45° angle).

In addition, calibration based on the measurement of a single point is also used. This is done for a known point in space. A measurement of the point in different configurations of the manipulator position is performed.

Another method is the comparison method [5]. It involves determining the deviations from the value of the calibrated element. The main element consists of several balls arranged side by side, which were calibrated on the coordinate measuring machine, then, the measuring arm measures the objects and the mutual distances from each other, and on this basis, the error from the nominal value is determined.

A similar method to the length measurement calibration method is the multi-position method [2]. It is described in detail in the paper TC13/WG10/ISO in Ref. [3]. The method is based on examining a given feature of the workpiece several times by changing the position three

* Corresponding author.
E-mail addresses: 216479@edu.p.lodz.pl (A. Bryszewski), 219181@edu.p.lodz.pl (J. Głowacki), piotr.zgorniak@p.lodz.pl (P. Zgórniak), leszek.podsedkowski@p.lodz.pl (L. Podsędkowski), agnieszka.kobierska@p.lodz.pl (A. Kobierska).

https://doi.org/10.1016/j.precisioneng.2023.07.002
Received 23 September 2022; Received in revised form 19 June 2023; Accepted 3 July 2023
Available online 13 July 2023

times around the X, Y, and Z axes. The workpiece also has measuring spheres.

Other methods use cameras or lasers, among others, to calibrate the measurement arms [3,4,19,21]. One work used a Nikon MV-200 laser [9] to calibrate a displacement sensor. Laser tracers are also used very frequently [10,11,13,15,16,18,24]. These sensors are used for Hand-Eye Calibration [12]. An interesting solution using a laser tracer is calibration based on an erroneous position model [20]. Hand-eye calibration of a robot is used to obtain the sensor's coordinate system relative to the robot's end. Many works used cameras and corresponding labels/markers to calibrate robots [14]. Another optical calibration method is optoelectronic measurement systems (OMS) [17]. A similar method is the Optical Tracking System, but it uses additional markers placed on the robot [22]. Other authors also proposed using a scanner and three balls for calibration [26].

A novel way to calibrate industrial robots is a device called TriCal [23]. It is a portable, inexpensive, and wireless device mounted on an effector. The procedure involves moving the effector in such a way that the center point of the robot's tool matched the center of the four spheres in the device.

Another method is to calibrate two robots through the process of manipulator cooperation [25]. This is a significantly different approach from other methods and requires two robots.

The arm/robot calibration method presented in Ref. [6] uses a device called a ballbar and two bases. One base is attached to the robot's effector, while the other is stationary at the robot's base. The arrangement of the device and the bases forms a kind of hexapod that provides 72 positions when the ballbar is repositioned. The measurement method involves moving the robot in such a way as to rotate the robot's effector around the ballbar's bottom end, as the device has a nominal length of 150 mm and only measures a deviation of 1 mm. However, this method is lengthy and comes at a high cost, as the device itself costs about $13,000.

Recent methods of robot calibration are mixed methods and ones using advanced optimization algorithms [27–31]. The paper [27] describes calibration using a Leica AT960 laser tracker and a two-stage optimization algorithm. In the first stage, the least-squares method identifies the geometric parameters of the model, and in the second, least-squares support vector regression is used to compensate for the residual positioning error caused by non-geometric errors. The paper [28] uses the measurement of distances acquired by pull wire sensors, identification of geometric parameters, and nonlinearities using the Extended Kalman Filter and Regularized Particle Filter. In Ref. [29], the authors use Faro vantage laser tracker and identification using the submodels with equalized singular values. In Ref. [30], the authors use the laser tracker, the RMS method to determine the model parameters, and the Artificial Neural Network to correct the residuals. In Ref. [31], the authors use a laser tracker and axis-invariant theory.

All of the above methods work well when the measuring arm has actuators. In the absence of actuators, these methods are not effective, as they require moving the measuring probe automatically. Moving the manipulator by the operator can introduce an additional random factor that disrupts the calibration process. For this reason, the idea was to create a calibration station with two Stewart platforms capable of moving both the effector and the base of the manipulator in an automatic manner.

1.2. Novelty

The calibration stand is designed to calibrate the NaviFast6D measuring arms (Fig. 1), which fundamentally differ from those used in classical metrology tasks. This arm is designed for intraoperative surgical measurements, where both the base and the effector can move during the measurement. In addition, measurement with the arm includes both the position and orientation of the effector relative to the base [32–34].

Fig. 1. NaviFast6D used for hip joint measurement [32,33].

The key innovations compared to current stands and methods are as follows:

- Ability to reposition the base and effector of the measuring arm
- Alignment change in all degrees of freedom - 3 DOF of position and 3 DOF of orientation for both platform and effector
- Calibration based on six equations for each calibration position
- Fully automated measurement, without human intervention
- The measuring station has a positioning repeatability of 2.5 μm for linear measurements and $0.025\text{-}10^{-3}$ rad for angular measurements based on the repeatability test conducted [results - Table 5].
- The cost of building the stand is small.

2. Materials and methods

The following section will present a methodology for designing the stand with an indication of the detailed relationships that allow the stand parameters to be determined depending on the parameters of the measuring arm to be calibrated. This approach will allow readers to replicate the design process with the customization of the calibration stand parameters for a specific calibrated arm.

2.1. Selection of kinematics

The design work on the NaviFast6D measuring arm calibration station began with the selection of suitable kinematics for the device. It was to ensure high rigidity of the system, repeatability, backlash-free, and a simple design that does not create unwanted errors affecting repeatability. The designed measuring arm calibration station is dedicated to a specific NaviFast6D arm manipulator. However, it is possible to consider other types of measuring arms. Key to the selection of kinematics is the range of motion of the measurement manipulator. In the case of the NaviFast6D arm, this range is limited both by its operating principle and application. The arm operates by measuring the angular position of joints based on reading the direction of the gravity vector from adjacent sections [32]. For this reason, the range of angular motion must be limited so that none of the joint axes aligns vertically.

An even greater limitation appears when analyzing the application. During the artificial hip joint implantation procedure, the used ranges of angular position changes of the NaviFast6D arm are $\pm 30^{\circ}$ for the base and last section, and the range of displacement is only about 60 mm. Details of the ranges of all sections are shown in Table 2.

Very often, the source of errors affecting repeatability is the guides

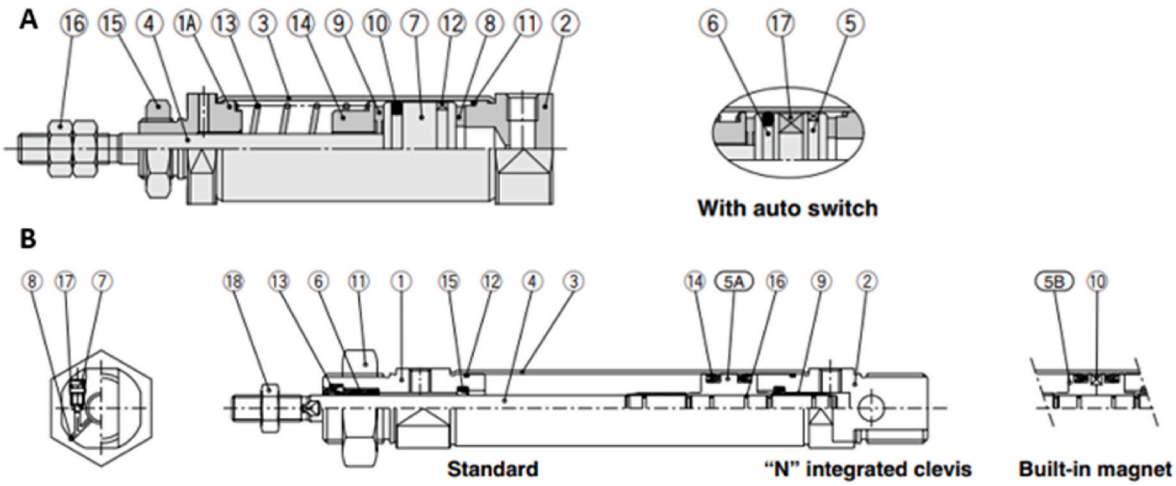

Fig. 2. Pneumatic actuators: **A** - Single-acting actuator with elastic damping SMC CDJ2E16-30SZ-B (where:1A-rod cover, 2- head cover,3- cylinder tube, 4- piston rod, 5- piston A, 6- piston B, 7- piston, 8-bumper A, 9-bumperB, 10 - piston seal, 11 - tube gasket, 12 - wear ring, 13 - return spring, 14 - spring seat, 15 - mounting nut, 16 - rod end nut, 17- magnet); **B** - Double-acting actuator with pneumatic damping SMC CD85N16–30C–B (where:1-rod cover, 2- head cover N, 3- cylinder tube, 4- piston rod, 5A-piston A, 5B- piston B, 6- bush, 7- cushion needle, 8-steel ball, 9-cushion ring, 10- magnet, 11- mounting nut, 12- tube gasket, 13-rod seal, 14- piston seal, 15-check seal, 16-piston gasket and cushion ring gasket, 17-needle seal 18- rod end nut). Detailed data in the technical documentation [7,8].

Table 1
Summary of the standard deviation of the tested actuators.

	Double-acting actuator		Single-acting actuator	
	Retraction	Extension	Retraction	Extension
Standard deviation [μm]	2150	1445	3542	2452

Table 2
Angular and linear displacement ranges of a single platform based on typical displacements of the NaviFast6D arm.

Limit	X [mm]	Y [mm]	Z [mm]	Rotation around the X axis (Roll) [°]	Rotation around the Y axis (Pitch) [°]	Rotation around the Z axis (Yaw) [°]
Lower	−50	−50	50	−45	−25	−45
Upper	50	50	166	45	25	45

and associated bearings. For this reason, these elements were excluded from the created layout of the stand. Taking these arguments into account, it was decided that the best kinematics would be a parallel robot, specifically the Stewart Platform. The Stewart Platform design provides 6° of freedom, high rigidity, and therefore high positioning accuracy, and has a single type of drive, such as pneumatic actuators. It was decided to use positioning only in the final positions of the actuators, which means that only a discrete number of positions will be available for calibration. This is a system where the distances between individual points, resulting from the lengths of the individual actuators in the retracted/extended form, fully define the positioning of the workpiece. The selected kinematics is the best solution in terms of repeatability since it depends, in general, mainly on the repeatability of the actuators. In addition to the actuators, there are motion-transmitting components on the platform, these can be, for example, ball joints or precision Cardan joints, but the latter are significantly more expensive, and more backlash may be created. Backlash in ball joints is minimized due to their small size relative to the actuators and the entire platform. In addition, to eliminate backlash in the joints, a tight fit should be used in them.

Because of the need to move both the base and effector of the NaviFast6D arm, the stand should consist of two platforms. This will further ensure redundancy of possible positions and, as a result, much wider than minimal possibilities for calibration and testing of the measuring arm. Since there are a total of 12 actuators in two Stewart platforms, so $2^{12} = 4096$ calibration positions are available. The stand consisting of two platforms is shown in Fig. 9.

2.2. Selection of drives

The actuators are key components in the entire stand. Their repeatability of length in the retracted and extended end positions determines the final repeatability of the entire system. Due to the simple design of the actuators, the greatest influence on the repeatability of the actuators is the type of damping/amortization and the manufacturing quality of the face of the piston and the surface with which the piston meets. For this reason, it was decided to study two types of actuators:

- single-acting actuator with elastic damping (Fig. 2 – A).
- double-acting actuator with pneumatic damping and rigid bumper (Fig. 2 – B).

For this purpose, a test stand was built to check the repeatability of the end positions of the two types of actuators presented in Fig. 2.

The measurement method used consisted of setting the dial sensor to the tested position, then changing the piston rod's position to either retracted or extended and returning to the initial position. The number of repetitions of the actuator positions was 80. The fabricated test stand for testing the repeatability of pneumatic actuators is shown in Fig. 3. It consists of the following:

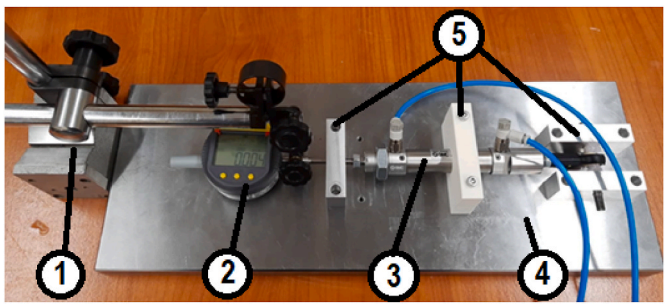

Fig. 3. Repeatability test stand. 1 - tripod for the sensor; 2 - TESA digital sensor; 3 - actuator under test; 4 - steel plate; 5 - mounting blocks.

- steel plate bases (4)
- actuator mounting blocks (5)
- TESA digital sensor (2) with 1 μm resolution with tripod (1).

The positions for the extended and retracted actuator were tested. The results in the form of deviation from the initial value for successive measurements are shown in Figs. 4 and 5. Due to the maximum permissible error (EMPE) of the digimatic indicator used, EMPE = 0.002 mm, in the experiments presented, it can be seen that the obtained scatter of the measured quantity can be the result of the measurement error of the digimatic indicator and the misaligned throttle-return valve on the actuators. The actuator should move quickly and slow down to the maximum at the final stage. It should be noted that this testing method was only to select a specific actuator design and was not used to determine the partial error used later to estimate the repeatability of the position of Stewart platforms.

Slightly better results were obtained for the double-acting actuator (Fig. 4) with pneumatic damping, probably due to the absence of rubber bumpers, so the surfaces always adhered to each other similarly. For this reason, it was decided to use a double-acting actuator with pneumatic damping (SMC CD85N16–30C–B) with a piston diameter of 16 mm and a stroke of 30 mm in the stand design. The values of the standard deviation are shown in Table 1 for actuators with structurally assured fixed piston rod orientation.

In addition, during testing, it was found that repeatability was affected by the angular orientation of the piston rod. Care had to be taken to ensure that the piston rod was always in the same angular orientation relative to the body during movement. This was an important finding, as the design of the Stewart Platform should take into account the proper locking of the movement around the axis of the piston rod.

2.3. Selection of the range of displacement to the requirements of the arm

The main way to get the right range of motion was to write an optimization program that selects design dimensions for 64 cases of platform arrangement. It was decided to look for four parameters, which are the retraction and extension of the actuator and the bottom and top radius of the circle (respectively C_{Base}, C_{p1}, and C_{p2} shown in Fig. 6) on which the joints connecting the actuators to the platform are placed.

In order to do this, a cost function was created, the minimization of which will result in the best solution. This function consists of two components - the cost function associated with exceeding/not exceeding the limits of the variables X, Y, and Z, rotation around the X/Y/Z axis (Roll, Pitch, Yaw), and the standard deviation function of the same variables. The limitations mentioned earlier are the ranges of variables X, Y, Z and rotation around the X/Y/Z axis (Roll, Pitch, Yaw) which are due to the design and size of NaviFast6D. These constraints were obtained through experiments on the 3D model of NaviFast6D and the measurements made while conducting surgical operations on the model stations. These constraints are within the constraints set in the theoretical analysis [32].

The ranges of variation of individual parameters were further divided into two due to the fact that the displacements of both platforms add up. The resulting constraints for a single platform are shown in Table 2.

With the constraints thus defined, it was possible to move on to defining a suitable cost function. This function must work on the basis of a simple kinematics task that calculates global coordinates based on the articulated coordinates, that is, the lengths of the individual actuators. Based on four parameters, which are the retraction and extension of the actuator and the bottom radius and top radius of the circle, the program calculates the coordinates of the center of the upper platform for 64 positions (6 actuators with two positions each => 2^6 = 64), and at this point, the program must calculate the cost associated with reaching the designated point. It was decided that the basis of the function would be the arctangent since its set of solutions is the range from (-π)/2 to π/2. It can be easily converted to 0–1 or only use the 0–1 range. The formula for cost is as follows:

$$\text{Cos tLimits}_{ij} = \frac{\arctan\left(q_{ji} - qll_j\right) + \arctan\left(qul_j - q_{ji}\right)}{\pi} \quad (1)$$

where:

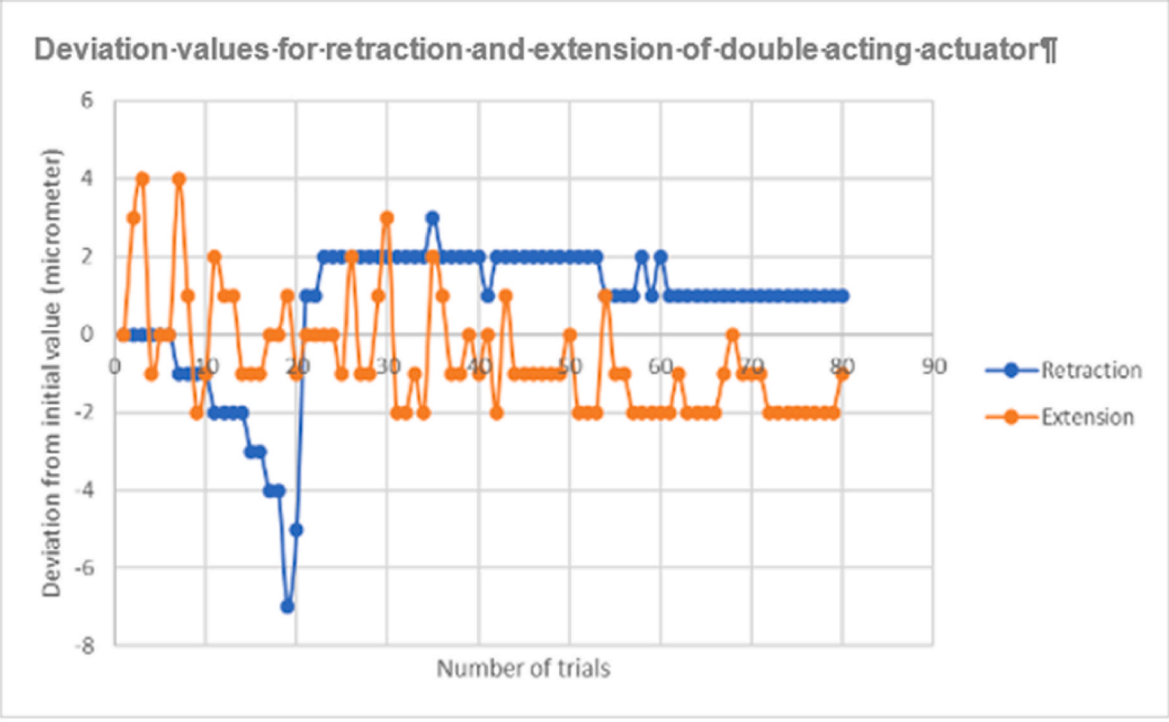

Fig. 4. Deviation values for retraction and extension of the double-acting actuator.

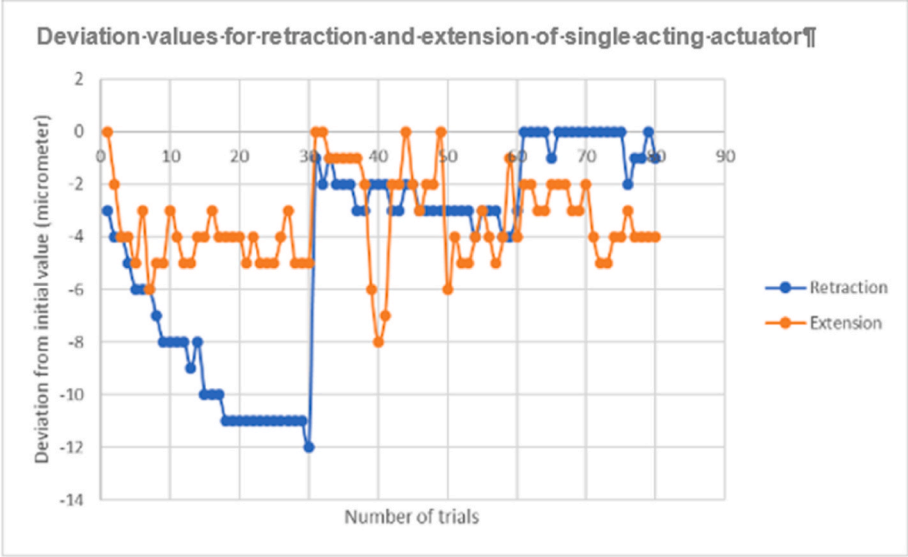

Fig. 5. Deviation values for retraction and extension of the single-acting actuator.

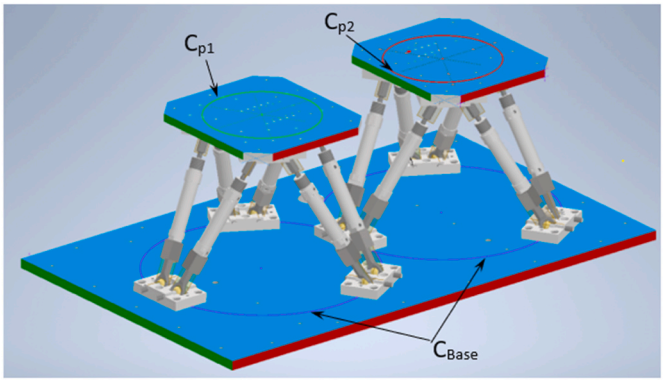

Fig. 6. Circles C_{Base}, C_{p1}, and C_{p2} on which the joints are connected to the lower base and upper platforms.

q_{ji}; $q_{ji} \in \{X_i, Y_i, Z_i, RotZ(Yaw)_i, RotY(Pitch)_i, RotX(Roll)_i\}$ – consecutive linear [mm] and angular [°] coordinates of the Stewart Platform [mm] for the *i* setting of the platform,
qll_j– *the value of the lower limit corresponding to a given global coordinate*,
qul_j– *the value of the upper limit corresponding to a given global coordinate.*

Equation (1) uses weights of 1/[mm] for displacement and 1/[°] for rotation due to the similar ranges of variation of those parameters (3 x displacement and 3 x rotation) in this particular solution. The graph of the function (formula 1) for the case $q_{ji} = X_i, Y_i$ is shown in Fig. 7. From the graph, it can be seen where the range ends. For the case of the X and Y axes, the values are −50 mm and 50 mm. The function returns a cost close to 1 only when the value of the coordinate is within this range. When the range is exceeded, the cost value decreases to 0.

After creating an overrun cost function, it was necessary to create another cost function related to the corresponding point spread, as there may be little or no movement of the platform if only one (previous) function is used. For this purpose, the standard deviation value of 64 platform positions in each of the six directions was used. Having already had the deviation values, as for the cost of the limits, arctangents were used as the basis function, and the formula for the cost associated with the spread of the points is as follows:

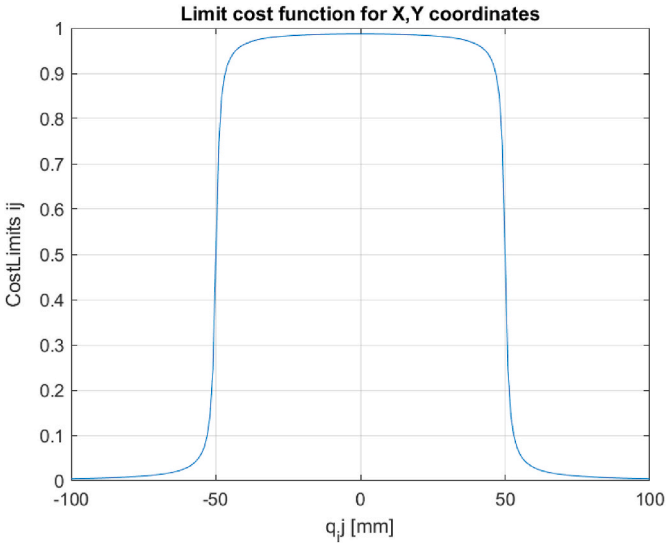

Fig. 7. Limit cost function for X, Y coordinates.

$$\mathrm{CostStd_j} = \frac{\arctan\left(\frac{6\sigma_{q_j}}{\mathrm{qul_j} - \mathrm{qll_j}}\right)}{\frac{\pi}{2}} \tag{2}$$

where:

σq_j - standard deviation value corresponding to a given global coordinate,
qll_j– the value of the lower limit corresponding to a given global coordinate,
qul_j– the value of the upper limit corresponding to a given global coordinate.

The 6σ value is derived from the Gaussian normal distribution graph (-3σ to 3σ). On the other hand, the whole function is divided by π/2 to obtain the value from 0 to 1. The graph of the above function for the X, Y coordinate range is shown in Fig. 8. The function is to return the cost associated with the standard deviation of the coordinates. The greater the standard deviation, the greater the cost. The highest possible cost

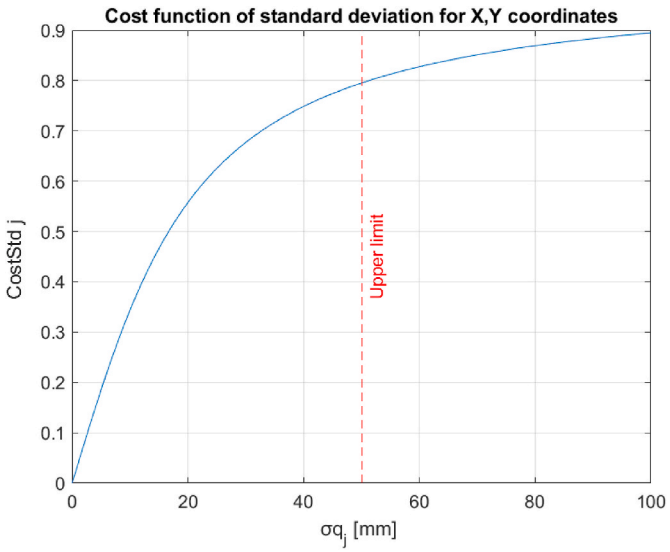

Fig. 8. Graph of the cost function associated with the standard deviation for X, Y coordinates.

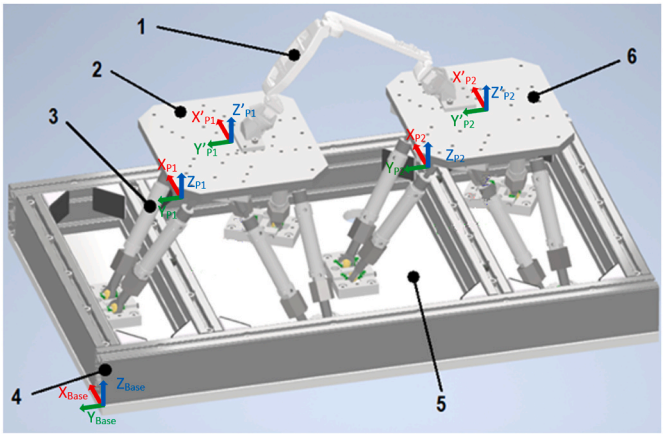

Fig. 9. NaviFast6D arm calibration test stand.

had to be achieved in both this function and the previous one.

The final step is to add up the two costs and optimize the total cost. A ready-made function in the MATLAB program "$f_{minsearch}$" was used for this purpose. This function finds the minimum of a function of multiple variables. In the case described here, the maximum was sought, so the total cost function should be taken with a minus sign. The function, based on the cost function, calculates the corresponding parameters, which are the retraction and extension of the actuator and the lower and upper radius of the platform.

$$\mathrm{Cost} = -\left(7 * \prod_{j=1}^{6} \mathrm{CostStd}_j + \frac{1}{64}\sum_{i=1}^{64}\prod_{j=1}^{6}\mathrm{CostLimits}_{ij}\right) \quad (3)$$

Based on the assumptions made and the optimization performed, the following values were obtained, as shown in Table 3. However, due to the lack of actuators of such dimensions in the commercial offer, the parameter values had to be modified. Parameters such as actuator stroke and bottom radius remained unchanged. The final values of the parameters are shown in Table 4.

For the platforms optimized in this way, the optimization of the spacing of the platforms and the foundation point of the base and effector of the measuring arm was accomplished analogously. The optimization criterion was to maximize the number of positions in which calibration can be carried out. As a result of the optimization, such a mounting of the arm and spacing of the platforms was established, for which only 123 out of 4096 possible calibration positions result in exceeding the rotation limits on the individual joints of the measuring arm.

Table 3
Parameters of the actuators and Stewart Platform obtained in the process of optimization of the total cost function.

Retraction [mm]	Extension [mm]	Actuator stroke [mm]	Lower radius [mm]	Upper radius [mm]
170	200	30	140	82

2.4. Construction

The calibration stand, together with the mountings and components discussed, is shown in Figs. 9 and 10. The main features that the calibration stand should have been high rigidity and repeatability of platform positioning and simple technological implementation. In this stand, the bearing arrangement has been minimized by not having rotating shafts. The element that fixes the drives and transmits motion is the articulated heads (8), which are the only rotating element. The stand also has very rigid, uniform mounts (10) in which the heads (8), flexible pin (11), and bushings (9) are seated. The bushings (9) were designed to eliminate axial backlash once the heads are seated on the stud.

The connections shown were made in a tight fit to fully prevent any backlash. Appropriate notches are used in the fasteners (10) to prevent the pivot heads from rotating. The use of the appropriate thickness of the lower base (5) and upper platforms (2,6) and the use of additional aluminum profiles (4) also had a large impact on increasing rigidity.

3. Repeatability measurements

In this chapter, the method of measuring the repeatability of the test stand will be presented and described. Then the results will be presented and discussed.

3.1. Measurement method

The repeatability test was carried out using a DEA Global Performance Coordinate Measuring Machine (CMM) with the technical specifications shown in Fig. 12(b). This method of measurement guarantees the rigidity of the measurement system, and it is an efficient method (two platforms in all degrees of freedom are measured during one measurement). Thanks to the possibility of programming the movements of the CMM, measurements can be performed repeatedly in a reproducible manner. Linear and angular deviations in each platform's three X, Y, and Z axes were checked. The measurement station is shown in Fig. 12(a).

The repeatability measurement first consisted of measuring three planes of the lower base (5), using which a coordinate system $X/Y/Z_{Base}$ and a base point was determined, which took the coordinates [0 0 0] for subsequent measurements. Next, the three upper planes of platforms 1 and 2 were measured (Fig. 11).

The platforms were tested in a position where all actuators were extended. The test position was reached from the position where all actuators are retracted. Fifteen repetitions were performed. Another 15 repetitions were made from random positions. Each plane was measured based on four points (Fig. 12(c)).

Table 4
Final parameters of the actuators and Stewart Platforms.

Retraction [mm]	Extension [mm]	Actuator stroke [mm]	Lower radius [mm]	Upper radius [mm]
193	223	30	140	65

Table 5
Standard deviation values for repetitions from access from one direction and from a random direction.

	Standard deviation					
	Platform 1					
Direction from	X [μm]	Y [μm]	Z [μm]	Rotation around [10^-3 rad]		
				X axis	Y axis	Z axis
One position	0.5	0.6	0.5	0.003	0.001	0.002
Random position	2.1	2.0	0.9	0.020	0.025	0.016
	Platform 2					
Direction from	X [μm]	Y [μm]	Z [μm]	Rotation around [10^-3 rad]		
				X axis	Y axis	Z axis
One position	0.4	1.0	0.4	0.009	0.004	0.002
Random position	1.5	2.5	0.6	0.014	0.019	0.024

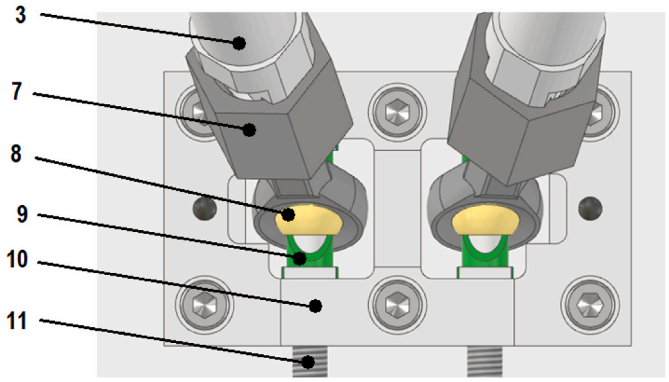

Fig. 10. Fastening of joints on the calibration test stand.

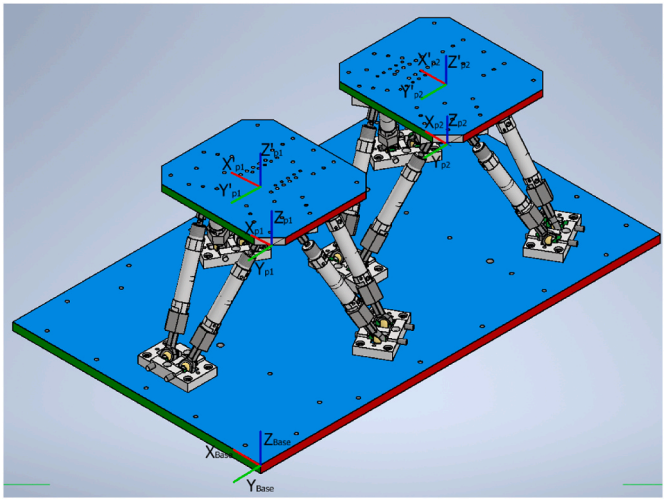

Fig. 11. Three planes of the lower base and the three planes of the upper platforms 1 and 2 (blue (Z = 0 plane), red (X = 0 plane), and green (Y = 0 plane)). (For interpretation of the references to colour in this figure legend, the reader is referred to the Web version of this article.)

After the measurements were taken, the equations of the planes had to be created from the collected data. Then, for each of the upper platforms (2, 6) and the lower base (5), a unit vector from the largest plane was selected as the initial one, and then two more unit vectors perpendicular to the previous one and to each other were created.

Based on the unit vectors and the intersection point of the three planes, a transform matrix was created from the base point (the origin of the coordinate system $X/Y/Z_{Base}$) to the intersection point of the three planes (origin of the coordinate system $X/Y/Z_{P1}$ and origin of the coordinate system $X/Y/Z_{P2}$ shown in Fig. 11). The final step was to move the measuring point of the upper platforms to the center of the coordinates of the given platform (e.g., from the origin of the coordinate system $X/Y/Z_{P1}$ to the origin of the coordinate system $X'/Y'/Z'_{P1}$). This was done by multiplying the transforms by the linear shift transform, which is known by construction.

3.2. Test results

The results of the platform repeatability tests are presented in boxplots in Figs. 13–16. A box plot provides a visualization of summary statistics for sample data and contains the following features: the bottom and top of each box are the 25th and 75th percentiles of the sample, respectively. The distance between the bottom and top of each box is the interquartile range. The red line in the middle of each box is the sample median. If the median is not centered in the box, the plot shows sample skewness. The whiskers are lines extending above and below each box. Whiskers go from the end of the interquartile range to the furthest observation within the whisker length (the *adjacent value*). Observations beyond the whisker length are marked as outliers. By default, an outlier is a value that is more than 1.5 times the interquartile range away from the bottom or top of the box. An outlier appears as a red + sign. The graphs in Figs. 13 and 14 show the results of tests from the first 15 trials, i.e., accesses occurred from a single position, while the graphs shown in Figs. 15 and 16 are the results of platform repeatability tests for accesses that occurred from random positions.

Figs. 13 and 15 show the deviation from the mean value of the linear coordinates of the center of the upper platforms, while Figs. 14 and 16 show the deviation from the mean value of the angular coordinates.

The standard deviations determined from the collected measurements are shown in Table 5. Repeatability measurements were also carried out for the lower position of the platforms - all actuators retracted. The standard deviations determined from them were similar to those with all actuators extended. The resulting position of the platforms depends on the length of all six actuators, and this also applies to the rotation of the platforms, so if the length of the individual actuators in either the extended or retracted positions were not repeatable, this would result in a change and lack of repeatability of both linear and angular positions. For this reason, it does not matter which set of positions we choose to measure repeatability as long as it includes all the actuators' retracted and extended positions.

Based on the high repeatability obtained for both the lower and upper positions of all actuators, it can be concluded that the repeatability will be analogous for each of the other platform positions.

At the end of the repeatability tests, measurements of the position of the upper platforms relative to the lower base were carried out for each of the $2^6 = 64$ arm actuator extension combinations. The measurements were performed independently for each platform. However, since the target stand will calibrate arms with the base placed on one platform and the effector on the other platform, this gave $64 \times 64 = 4096$ possible arm positioning combinations from which those on which calibration may be performed can be selected.

4. Discussion

The research presented in the article provides new insights into the link between the repeatability of a manipulator and the tasks it faces.

The positioning accuracy of the calibration device is crucial for the task of calibrating measuring equipment. As a standard, it should be an order of magnitude higher than the accuracy of the device being calibrated. Surgical procedures and implants used in artificial hip joint implantation allow adjustment in 3 mm increments, so a measurement accuracy of 0,5 mm was assumed to be fully sufficient. In the case of the NaviFast6D measuring arm, its accuracy is not yet known, so it was assumed that the calibration device would have the highest possible repeatability at a reasonable cost. Determination of the actual coordinates of the calibration device is carried out using a CMM with a

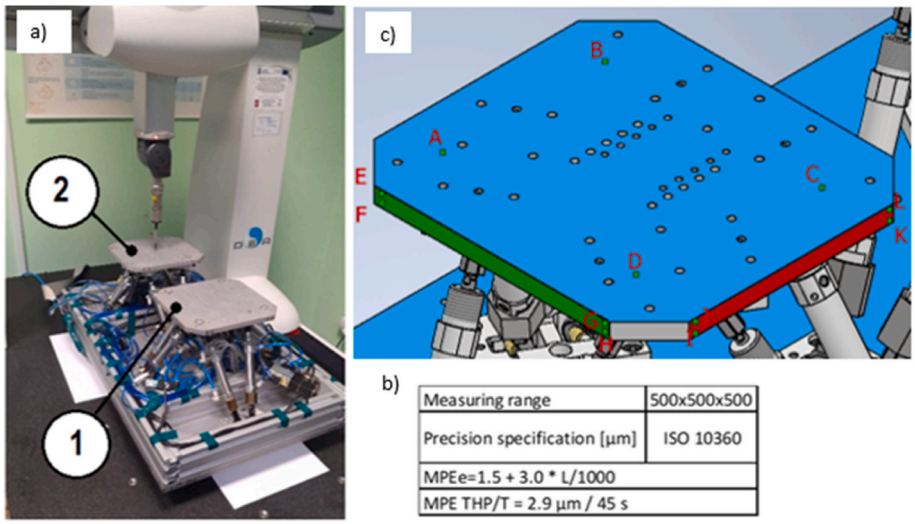

Fig. 12. a) Stewart Platform repeatability test stand (1, 2) on the CMM; b) Technical parameters of the DEA Global Performance CMM, c) –The points for measurement of planes of the upper platform: ABCD – for Z = 0 plane, EFGH for Y = 0 plane and IJKL for X = 0 plane (P1).

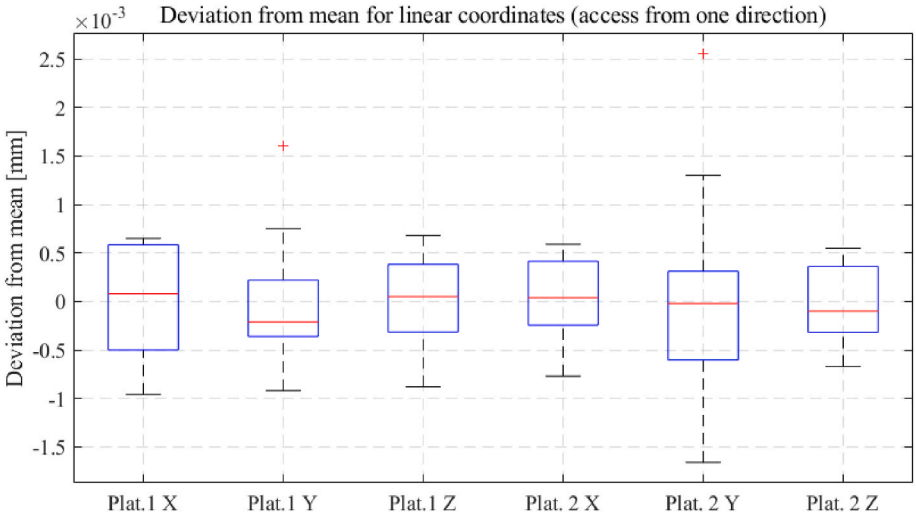

Fig. 13. Graph of the deviation from the mean value of the linear coordinates of the center of the upper platforms (access from one direction).

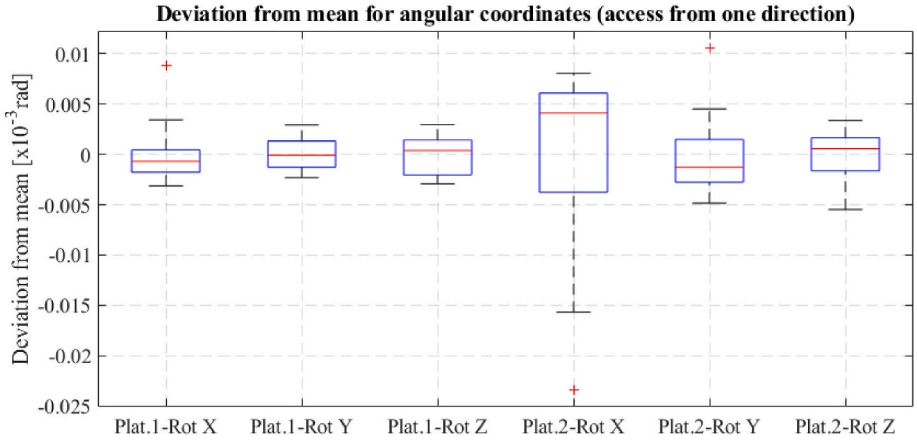

Fig. 14. Graph of the deviation from the mean value of the angular coordinates of the platforms (access from one direction).

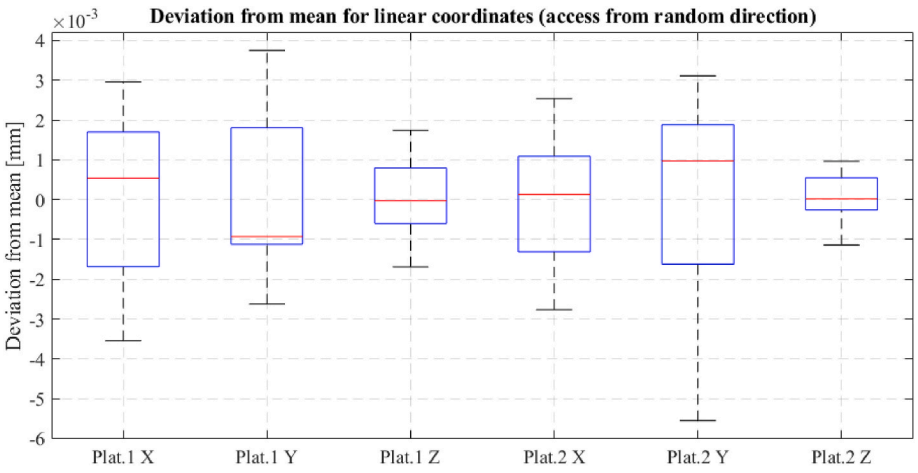

Fig. 15. Graph of the deviation from the mean value of the linear coordinates of the center of the upper platforms (access from a random direction).

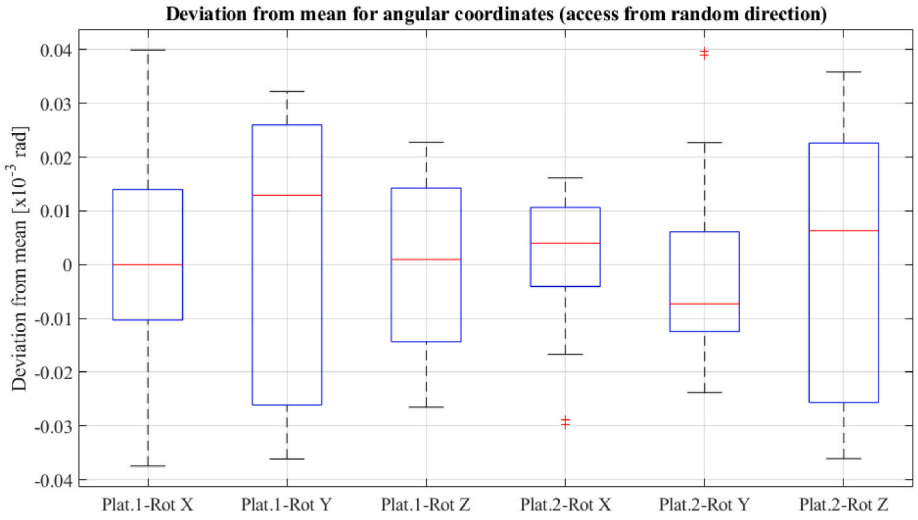

Fig. 16. Graph of the deviation from the mean value of the angular coordinates of the platforms (access from a random direction).

repeatability of 1.5 μm (based on the calibration certificate of the CMM machine), so it was decided that the repeatability of the calibration device should be at a similar level.

In the case of ordinary manipulators, positioning is most often required of them over the entire range of motion since the task facing the manipulator is not known at the design stage. In the case of calibration devices, a certain number of positions are usually required (several to dozens, depending on the type of manipulator). These positions must be spread over most of the working area of the device to be calibrated, but their specific settings can be arbitrary. For this reason, this article proposes a different approach to the design of calibration devices from the classical one. Classical precision systems use Cartesian manipulators driven by ballscrews, for which travel fluctuation over useful path v_{up} is min. 4 μm for the T0 class and 6 μm for the T1 class (according to Hiwin catalog based on DIN ISO 3408 and JIS [35]). This shows that achieving the required accuracy at a reasonable cost will be impossible on such a machine, as it will require additional measuring systems. In contrast, using rigid bumper positioning (as in the presented solution - rigid bumpers are built-in limiters of the range of motion in the pneumatic cylinders) gives very good repeatability - at the expense of reducing the number of positioning points. However, using the kinematic structure of the Stewart platform allows 64 points with all six degrees of freedom variables. This number of positions is quite sufficient to calibrate any measuring arm, provided that these points are correctly distributed in the working space of the measuring arm. The use of two platforms already gives 4094 relative positions, which provides a very large margin, slightly increasing the cost. To obtain the correct distribution of points, an optimization procedure was proposed to select the structural dimensions of the Stewart platform and match them to the requirements of a particular arm.

Another inconvenience appears here - the calibration device constructed in this way is matched only to one design of the measuring arm. However, if we take into account the low cost of building the platform (about $3000 with control) and the fact that it is used in the mass production of measuring arms, this inconvenience does not seem to be significant. An additional inconvenience is the need to measure all $2 \times 64 = 128$ calibration positions on the CMM, which is time-consuming. However, this is done only once immediately after the platform is assembled, and in this context is acceptable.

The repeatability test method using a CMM has many advantages. The main advantage is the ability to measure accurately and quickly. Thanks to the automation of the measurement process, the measurement was carried out in the same place every time, thus avoiding inaccuracies due to errors in the shape of the measured surfaces. The measurement program involved building the coordinate system associated with the stand base in a two-step manner. First in manual mode and finally in automatic mode. The program determined three planes for each platform (top, front, side), and based on their intersection, the positions of

the characteristic point of platform 1 and platform 2 were determined. Each measured plane of the platform was determined from four points in repeated positions. The reference system was built at the intersection of the base plane of the stand, the front plane XZ and the side plane YZ associated with the base to which the actuators were attached. Based on the input points used to determine the component planes of the platforms, the rotation angles of the platforms were calculated. This measurement procedure provided the ability to compare the Cartesian coordinates of the characteristic points and the rotation angles for the analyzed Stewart platform calibration positions.

In discussing the results, the standard deviation was used. The standard deviation values for all graphs are shown in Table 5. The analysis of the measurement data shows that for linear coordinates the standard deviation of the position of the origin of the coordinate system does not exceed 1 μm for access from one direction, which determines the repeatability of the calibration device at the assumed level. The standard deviation for angular coordinates did not exceed 0.009 10^{-3} rad. For access from a random position, the values were 3 μm and 0.025 10^{-3} rad, respectively.

In addition, it is worth noting that measurement errors can also arise as a result of the inaccuracy of the CMM. Based on the calibration certificate of the CMM machine, the obtained repeatability of measurements of the CMM was 1.5 μm performed in accordance with ISO 10360-2. It follows that the measured repeatability of the stand is close to that of the CMM machine. It is worthwhile to make a similar measurement in the future but with a more accurate CMM.

One of the limitations of the presented research is the lack of verification of the long-term stability of the calibration values. This will be the subject of further research on the device. When discussing the results obtained, it is also worth noting the rather significant, almost threefold difference in repeatability when accessing from the same direction and when accessing from different directions. This indicates that the design can be further optimized. As shown in preliminary measurements, the repeatability of actuator extension depends on the angular position of the piston along with the piston rod relative to the actuator body. The current design limits this angular movement but does not eliminate it completely. If higher requirements were placed before the calibration device, this angular motion would have to be eliminated completely. A second possible source of reduced repeatability could have been plastic spherical joints with fairly low accuracy. Replacing them with metal ones and making in a better class of accuracy would have improved results.

5. Conclusions

The aim of the project was to obtain a highly repeatable stand for calibrating the NaviFast 6D measuring arm. This was achieved by selecting linear dual-mode drives and the correct selection of design parameters derived from the optimization program, stiffening the entire design, eliminating as much backlash as possible, predicting the effect of piston rod rotation on repeatability and creating an appropriate constraint on this movement. In order to confirm repeatability, a suitable measurement method had to be selected. It was decided to measure with a CMM. The standard deviation of the linear position of the origin of the coordinate system in each direction in the stand repeatability tests is about 0.6 μm (Table 5), while the initial assumption was to obtain 1 μm. In addition, it is worth mentioning that this is a stand whose construction cost is relatively small compared to the results achieved.

It should also be noted that a stand consisting of two Stewart platforms can be perfectly suitable for calibrating not only the NaviFast6D but also other measuring arms. It is also possible to mount the measuring arm at different points on the platforms as needed. This is an innovative way to calibrate arms also because the base and effector of the measuring arm can be changed, and the measurement and calibration are fully automatic.

The work was funded under Project No. **POIR.01.01–00–0290/21** by the Polish National Centre for Research and Development.

Declaration of competing interest

The authors declare that they have no known competing financial interests or personal relationships that could have appeared to influence the work reported in this paper.

References

[1] EN ISO 10360-12. Geometrical product specifications (GPS) – Acceptance and reverification tests for coordinate measuring systems (CMS) Part 12. Articulat Arm Coordinate Measurement Mach (CMM) 2016.
[2] Ksenia Ostrowska Redundantywne współrzędnościowe systemy pomiarowe – modelowanie matematyczne i funkcjonalne. Monografie Politechniki Krakowskiej. Seria Mechanika 2018.
[3] Marek P, Piszczek Ł. Testing of an industrial robot's accuracy and repeatability in off and online environment. Eksploat. Niezawodn. Maint. Reliab. 2018.
[4] Albert N, Bonev I. Absolute calibration of an ABB IRB 1600 robot using a laser tracker. Robot. Comput. Manuf. 2013.
[5] ISO/CD TS 15530-2 GPS use of multiple measurement stratige.
[6] Nubiola A, Bonev I. Absolute robot calibration with a single telescoping ballbar. Precis Eng 2014.
[7] https://www.smcpneumatics.com/CDJ2D16-30SZ-B.html. Actuator technical documentation SMC CDJ2E16-30SZ-B.
[8] https://www.smcpneumatics.com/CD85N16-30C-B.html. Actuator technical documentation SMC CD85N16-30C-B.
[9] Kim Yong-Sik, Dagalakis Nicholas, Marvel Jeremy, Cheok Geraldine. Design and testing of wireless motion gauges for two collaborative robot arms. Meas Sci Rev 2022;22:84–91. 10.2478.
[10] Luo Jingbo, Chen Silu, Fan Xiaonan, Xiong Ciyuan, Zheng Tianjiang, Zhang Chi, Yang Guilin. Kinematic calibration of a 4PPa-2PaR parallel mechanism with subchains on limbs. IEEE Trans Instrum Meas 2022;71:750211. https://doi.org/10.1109/TIM.2022.3156998.
[11] Stepanova Karla, Rozlivek Jakub, Puciow Frantisek, Krsek Pavel, Pajdla Tomas, Hoffmann Matej. Automatic self-contained calibration of an industrial dual-arm robot with cameras using self-contact, planar constraints, and self-observation. Robot Comput Integrated Manuf 2022;73:102250. https://doi.org/10.1016/j.rcim.2021.102250.
[12] Gao Yongzhuo, Gao Haibo, Bai Kunpeng, Li Mingyang, Dong Wei. A robotic milling system based on 3D point cloud. Machines 2021;9:355. https://doi.org/10.3390/machines9120355.
[13] Boby Riby, Klimchik Alexandr. Combination of geometric and parametric approaches for kinematic identification of an industrial robot. Robot Comput Integrated Manuf 2021;71:102142. https://doi.org/10.1016/j.rcim.2021.102142.
[14] Boby Riby. Identification of elasto-static parameters of an industrial robot using monocular camera. Robot Comput Integrated Manuf 2022;74:102276. https://doi.org/10.1016/j.rcim.2021.102276.
[15] McGarry Lauren, Butterfield J, Murphy Adrian. Utilising industry 4.0 technologies to enhance robotic capability for aerospace assembly. 2021.
[16] Zhang Ying, Qiao Guifang, Song Guangming, Song Aiguo, Wen Xiulan. Experimental analysis on the effectiveness of kinematic error compensation methods for serial industrial robots. Math Probl Eng 2021;2021:1–9. https://doi.org/10.1155/2021/8086389.
[17] Cornagliotto Valerio, Digo Elisa, Pastorelli Stefano. Using a robot calibration approach toward fitting a human arm model. 2021. https://doi.org/10.1007/978-3-030-75259-0_22.
[18] Shen Huiping, Meng Qingmei, Li Ju, Deng Jiaming, Wu Guanglei. Kinematic sensitivity, parameter identification and calibration of a non-fully symmetric parallel Delta robot. Mech Mach Theor 2021;161:104311. https://doi.org/10.1016/j.mechmachtheory.2021.104311.
[19] Boby Riby. Kinematic identification of industrial robot using end-effector mounted monocular camera bypassing measurement of 3D pose. IEEE ASME Trans Mechatron 2021. https://doi.org/10.1109/TMECH.2021.3064916. 1-1.
[20] Chen Tianyan, Lin Jinsong, Wu Deyu, Wu Haibin. Research of calibration method for industrial robot based on error model of position. Appl Sci 2021;11:1287. https://doi.org/10.3390/app11031287.
[21] Jian Sheng, Yang Xiansheng, Yuan Xianwei, Lou Yunjiang, Jiang Yao, Chen Genliang, Liang Guoyuan. On-line precision calibration of mobile manipulators based on the multi-level measurement strategy. IEEE Access 2021. https://doi.org/10.1109/ACCESS.2021.3053356. 1-1.
[22] Liu Ying, Li Yuwen, Zhuang Zhenghao, Tao Song. Improvement of robot accuracy with an optical tracking system. 2021. https://doi.org/10.37247/PASen.2.2021.3.
[23] Icli Caglar, Stepanenko Oleksandr, Bonev Ilian. New method and portable measurement device for the calibration of industrial robots. Sensors 2020;20:5919. https://doi.org/10.3390/s20205919.
[24] Wang Xuhao, Zhang Dawei, Zhao Chen, Guo Zhiyong, Wu Mengli, Meng Xiangzhi, Ma Li. Kinematic calibration of a 7R 6-DOF robot with non-spherical wrist using laser tracker. 2020. https://doi.org/10.21203/rs.3.rs-60243/v1.
[25] Gan Yahui, Dong Donghui. Robot calibration for cooperative process under typical installation. J Appl Math 2014;2014:1–12. https://doi.org/10.1155/2014/576420.

[26] Tian Yaming, Xiong Jie, Wang Gang, Jiang Cheng, Zhang Sheng, Li Wenlong. A novel position and orientation correction method for specific robot poses by measuring an array of standard balls. Meas Sci Technol 2021;32. https://doi.org/10.1088/1361-6501/ac2a67.
[27] Bm Ming, Zhang Minglu, Zhang He, Manhong Li, Zhao Jie, Chen Zhigang. Calibration method based on models and least-squares support vector regression to enhance robot positioning accuracy. IEEE Access 2021. https://doi.org/10.1109/ACCESS.2021.3115949. 1-1.
[28] Gao Guanbin, Li Yuan, Liu Fei, Han Shichang. Kinematic calibration of industrial robots based on distance information using a hybrid identification method. Complexity 2021;2021:1–10. https://doi.org/10.1155/2021/8874226.
[29] Jiang Zhouxiang, Huang Min. Stable calibrations of six-DOF serial robots by using identification models with equalized singular values. Robotica 2021;39:1–22. https://doi.org/10.1017/S0263574721000229.
[30] Hsiao Jenchung, Shivam Kumar, Lu Ifang, Kam Taiyan. Positioning accuracy improvement of industrial robots considering configuration and payload effects via a hybrid calibration approach. IEEE Access 2020. https://doi.org/10.1109/ACCESS.2020.3045598. 1-1.
[31] Xiao Pengfei, Ju Hehua, Li Qidong, Meng Jijun, Chen Feifei. A new fixed axis-invariant based calibration approach to improve absolute positioning accuracy of manipulators. IEEE Access 2020. https://doi.org/10.1109/ACCESS.2020.3011328. 1-1.
[32] Kobierska A, Rakowski P, Podsędkowski L. Modelling and testing the measurement repeatability of linear and angular positions of a measuring arm (miniature NaviFAST 6D device) Measurement MEAS-D-21-06318R1. 2022.
[33] Kobierska A, Rakowski P, Podsędkowski L. "Estimation of orientation and position of the manipulator using the extended Kalman filter based on measurements from the accelerometers" Journal of Automation. Mobile Robot. Intelligent Syst. 2019.
[34] Rakowski P, Kobierska A, Podsędkowski L, Poryzała P. "Accuracy and repeatability tests on 6D measurement arm" mechanics and mechanical engineering, vol. 21; 2017. p. 425–43. 2.
[35] https://www.hiwin.pl/Ballscrews&Accessories. [Accessed 20 August 2022]. BS-08-10-EN-2206-K online.